Analysis of Subgrid-Scale Closure Models for LES of Transcritical LOX-GCH4

By W. T. Chung AND M. Ihme

Department of Mechanical Engineering, Stanford University
Stanford, CA 94305, USA.

Simulations of rocket engines operating under high pressures that surpass the thermodynamic critical limit of the propellants require the consideration of complex fluid behaviors that pose challenges for numerical modeling and simulations. This study aims at assessing and ultimately improving the accuracy of subgrid-scale (SGS) models in large-eddy simulations (LES) for liquid rocket engine combustors. To this end, direct numerical simulations (DNS) of a transcritical LOX/GCH4 inert flow is performed. Using this data, *a priori* analysis is performed on the Favre-filtered DNS data to examine the accuracy of conventional SGS-models for predicting these high-pressure conditions. SGS terms calculated with the Vreman SGS model showed poor correlations with filtered DNS data. In contrast, SGS terms evaluated with the Gradient model showed improved agreement with the filtered DNS terms. Further analysis showed that SGS stress terms in the simulated transcritical flows demonstrated behavior that deviates from the eddy-viscosity hypothesis.

1. Introduction

The development of accurate computational tools is crucial in reducing the cost and development cycle of liquid rocket engines (LRE). Large-eddy simulations (LES) provide a feasible computational approach in capturing the behavior of flows within a rocket engine combustor. However, LREs involve the injection of cryogenic propellants into a rocket thrust chamber that is operating under conditions that exceed the thermodynamic critical limits of the rocket propellants. Consequently, LREs generate trans- and supercritical flows – with complex behaviors that pose challenges for numerical modeling and simulations. One such challenge in LES is the validity of applying existing subgrid-scale (SGS) models that have been typically developed for applications in subcritical flows [1, 15]. In particular, the introduction of non-ideal gas dynamics and supercritical thermodynamics, in LRE combustion simulations, casts doubt on the validity of such models.

Selle *et al.* [5] performed an *a priori* study of DNS data of three-dimensional two-species non-reacting supercritical mixing layers. The orders of magnitude of unclosed terms in the LES equations were evaluated using the DNS data; results showed that previously neglected unclosed terms for pressure and heat flux in the LES equations became essential under supercritical conditions. Values for turbulent SGS fluxes were also computed using three commonly-employed SGS models, and then compared with the exact terms from the DNS. Results showed that the values from the Smagorinsky model had poor correlation with the DNS data, whereas results from the Gradient model and Scale-similar model had good correlation.

Ribert *et al.* [12] employed *a priori* analysis on fully-compressible one-dimensional and three-dimensional DNS of turbulent ideal-gas hydrogen-oxygen flames to show that significant errors can arise from neglecting unclosed terms from the filtered the equation of state (EoS). In simulations of trans- and supercritical flows, these errors can become more significant due to stronger non-linearities that arise from filtering the real-gas EoS [5].

The SGS terms in the LES governing equations clearly require a closer inspection, in order to improve the accuracy of simulating flows inside LRE combustors. Hence, the objective of this study is to generate DNS data under LRE conditions and gain insight into the validity of SGS models for the representation of turbulent fluxes in LES of supercritical flows.

2. Method

The governing equations that are solved in the present study are the conservation equations for mass, momentum, energy, and chemical species:

$$\partial_t \rho + \nabla \cdot (\rho \boldsymbol{u}) = 0 \tag{2.1}$$

$$\partial_t (\rho \boldsymbol{u}) + \nabla \cdot (\rho \boldsymbol{u}\boldsymbol{u}) = -\nabla \cdot (p\boldsymbol{I}) + \nabla \cdot \boldsymbol{\tau}_v \tag{2.2}$$

$$\partial_t (\rho e) + \nabla \cdot [\boldsymbol{u}(\rho e + p)] = \nabla \cdot [(\boldsymbol{\tau}_v) \cdot \boldsymbol{u}] - \nabla \cdot \boldsymbol{q}_v \tag{2.3}$$

$$\partial_t (\rho \boldsymbol{Y}_k) + \nabla \cdot (\rho \boldsymbol{u} \boldsymbol{Y}_k) = -\nabla \cdot \boldsymbol{j}_{k,v} \tag{2.4}$$

with density ρ, velocity vector $\boldsymbol{u}$, pressure p, specific total energy e, stress tensor $\boldsymbol{\tau}$, and heat flux $\boldsymbol{q}$. $\boldsymbol{Y}_k$ and $\boldsymbol{j}_k$ are the mass fraction and diffusion flux for species k.

In the *a priori* analysis carried out in this study, a top-hat filter G with a desired filter size $\overline{\Delta}$ is applied on a arbitrary quantity ϕ from the DNS data:

$$\overline{\phi(\boldsymbol{x})} = \int_V \phi(\boldsymbol{x}) G(\boldsymbol{x} - \boldsymbol{y}) d\boldsymbol{y} \tag{2.5}$$

$$G(\boldsymbol{x} - \boldsymbol{y}) = \begin{cases} \frac{1}{\overline{\Delta}} & |\boldsymbol{x} - \boldsymbol{y}| \leq \frac{\overline{\Delta}}{2} \\ 0 & \text{otherwise} \end{cases} \tag{2.6}$$

and Favre-averaged:

$$\widetilde{\phi} = \frac{\overline{\rho\phi}}{\overline{\rho}} \tag{2.7}$$

After filtering, the governing equations become:

$$\partial_t \bar{\rho} + \nabla \cdot (\bar{\rho} \widetilde{\boldsymbol{u}}) = 0 \tag{2.8}$$

$$\partial_t (\bar{\rho} \widetilde{\boldsymbol{u}}) + \nabla \cdot (\bar{\rho} \widetilde{\boldsymbol{u}} \widetilde{\boldsymbol{u}}) = -\nabla \cdot (\bar{p}\boldsymbol{I}) + \nabla \cdot (\bar{\boldsymbol{\tau}}_v + \bar{\boldsymbol{\tau}}_{\text{SGS}}) \tag{2.9}$$

$$\partial_t (\bar{\rho} \widetilde{e}) + \nabla \cdot [\widetilde{\boldsymbol{u}}(\bar{\rho} \widetilde{e} + \bar{p})] = \nabla \cdot [(\bar{\boldsymbol{\tau}}_v + \bar{\boldsymbol{\tau}}_{\text{SGS}}) \cdot \widetilde{\boldsymbol{u}}] - \nabla \cdot (\bar{\boldsymbol{q}}_v + \bar{\boldsymbol{q}}_{\text{SGS}}) \tag{2.10}$$

$$\partial_t (\bar{\rho} \widetilde{\boldsymbol{Y}}_k) + \nabla \cdot (\bar{\rho} \widetilde{\boldsymbol{u}} \widetilde{\boldsymbol{Y}}_k) = -\nabla \cdot (\bar{\boldsymbol{j}}_{k,v} + \bar{\boldsymbol{j}}_{k,\text{SGS}}) \tag{2.11}$$

with subscripts v and SGS denote viscous and subgrid-scale quantities, respectively.

The Peng-Robinson cubic state equation is used to model real-fluid thermodynamics under transcritical conditions:

$$p = \frac{RT}{v - b} - \frac{a}{v^2 + 2bv - b^2} \tag{2.12}$$

with mixture specific gas constant R and specific volume v. The coefficients a and b

account for effects of intermolecular forces and volumetric displacement, and are dependent on temperature and composition [7]. Details regarding the evaluation of specific heat capacity, internal energy, and partial enthalpy from the Peng-Robinson state equation is described in Ma *et al.* [2].

Takahashi's high-pressure correction [6] is used to evaluate the binary diffusion coefficients. Since only two species are used in these inert simulations, the binary diffusion coefficients are exact. Thermal conductivity and dynamic viscosity are evaluated using Chung's method with high-pressure correction [4].

The unstructured compressible finite-volume solver Charles^x has been used to conduct the present simulation. In this solver, the convective fluxes are discretized using a sensor-based hybrid scheme [8] in which a fourth-order scheme is combined with a second-order scheme to describe sharp interfaces present in transcritical flows. Due to the density gradients present at trans- and supercritical conditions, an entropy-stable flux correction technique [2] is used to dampen non-linear instabilities in the numerical scheme. The double-flux method by Ma *et al.* [2, 3] is used to eliminate spurious pressure oscillations. A strong stability preserving 3rd-order Runge-Kutta (SSP-RK3) scheme is used for time integration.

3. DNS Setup and Initial Conditions

In the present study, DNS of an inert binary mixture is performed following the initial conditions summarized in Table 1. A pressure of 20 MPa was chosen to match liquid oxygen-gaseous methane (LOX-GCH4) rocket conditions, which can reach up to 25 MPa. Fuel and oxidizer temperatures, T_{CH4} and T_{O2}, of 300 K and 120 K respectively, are also typical for LOX-GCH4 engines.

$N_x \times N_y \times N_z$	Δ [μm]	$L_x \times L_y \times L_z$ [mm^3]	Re_t	l_τ [mm]	p [MPa]	T_{CH4} [K]	T_{O2} [K]
$256 \times 256 \times 32$	2.6	$0.625 \times 0.625 \times 0.0781$	200	0.0781	20	300	120

TABLE 1. Summary of DNS initial conditions.

The initial velocity profile was generated with a synthetic isotropic turbulence generator by Saad et al. [9, 13, 17] with zero mean velocity, based on the von Kármán-Pao energy spectrum:

$$E(\kappa) = \alpha \frac{u'^2}{\kappa_e} \frac{(\kappa/\kappa_e)^4}{[1 + (\kappa/\kappa_e]^{17/6}} \exp\left[-2\left(\frac{\kappa}{\kappa_\eta}\right)^2\right] \tag{3.1}$$

$$\alpha = 1.453 \tag{3.2}$$

$$\kappa_e = 0.746834/l_t \tag{3.3}$$

where u' is the RMS velocity, κ is the wave number, and κ_η the Kolmogorov wave number. The chosen scaling constant α and maximum energy wavenumber κ_e are typical for isotropic turbulence [11]. The integral lengthscale l_t and RMS velocity fluctuation u' have been chosen to produce a turbulent Reynolds number Re_t of 200 and an estimated Dahmköhler number Da of 380 for a reacting counterpart of the present inert DNS case. The Dahmköhler number is evaluated with the extinction strain rate of a one-dimensional

counterflow diffusion flame of a LOX-GCH4 mixture under similar conditions. Values for Da and Re_t correspond to the operating conditions of modern combustors following the regime diagram by Williams [14].

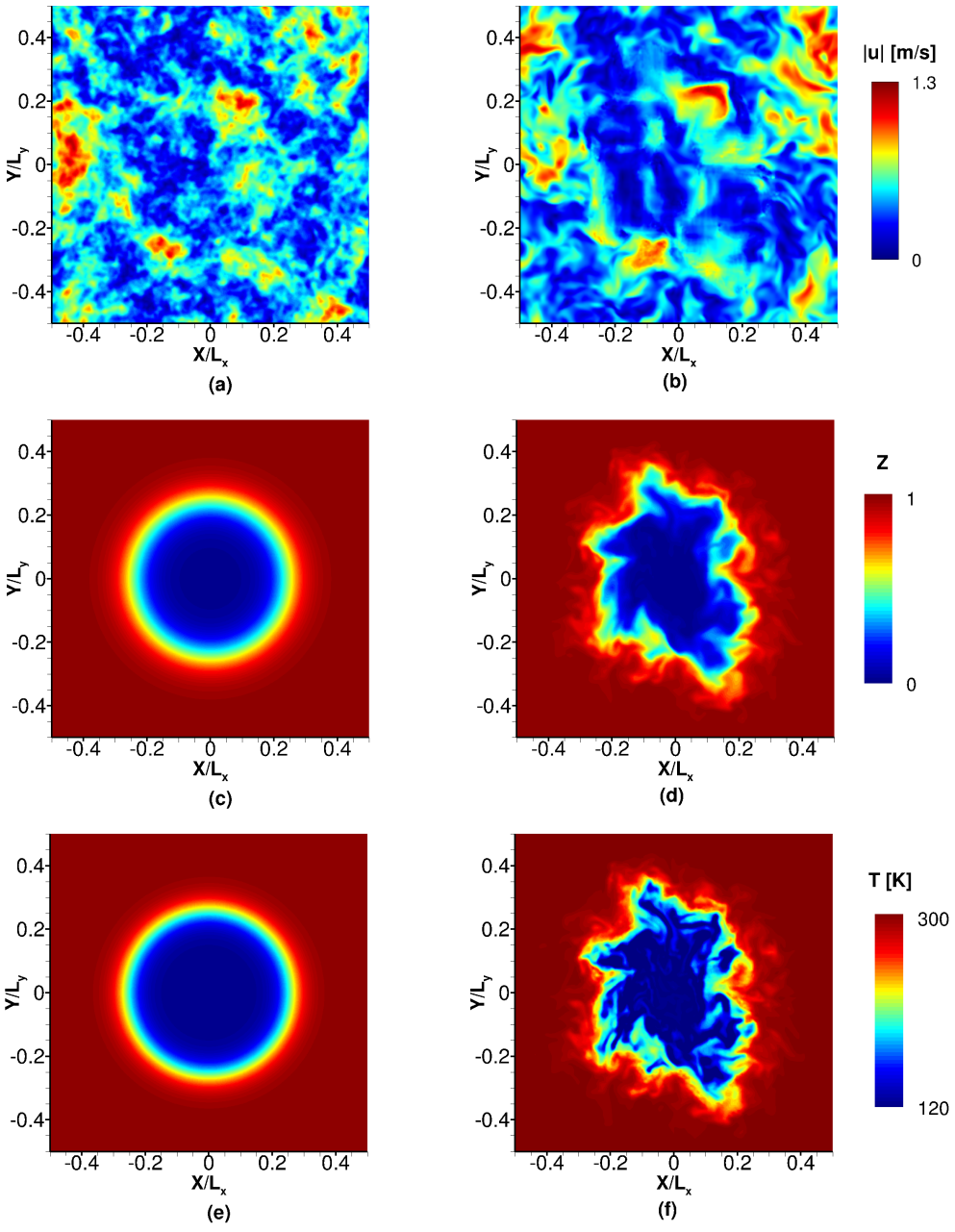

FIGURE 1. Cross-section of velocity magnitude, mixture fraction, and temperature at $t = 0$, in (a),(c), and (e) respectively, and $t = 0.12$ ms, in (b), (d), and (f) respectively.

The domain lengths in the x and y direction were chosen to be eight times the size of the integral lengthscale to minimize effects of the periodic boundary conditions. While it would be ideal to have a cubic domain, the length in the z direction has been reduced to one integral lengthscale to ensure feasible computational costs at two million cells. The cell size is prescribed at 2.6 μm, which is approximately twice the Kolmogorov lengthscale, in order to resolve all lengthscales.

After initialization, calculations were carried out until t = 0.06 ms when the velocity derivative skewness converges to a value of -0.5, which is indicative of realistic turbulence. The velocity derivative skewness Σ is given by:

$$\Sigma = \frac{\left\langle \left(\frac{\partial u}{\partial x} \right)^3 \right\rangle}{\left\langle \left(\frac{\partial u}{\partial x} \right)^2 \right\rangle^{3/2}} \tag{3.4}$$

where $\langle\rangle$ denotes the statistical average. Calculations were further carried out for an equal amount of time to allow mixing under realistic turbulent conditions, before *a priori* analysis is performed on the DNS data at 0.12 ms. The velocity magnitude, mixture fraction, and temperature at initialization is shown in figures 1(a), 1(c), and 1(e) respectively, and at 0.12 ms in figures in figures 1(b), 1(d), and 1(f) respectively. The mixture fraction Z for the present binary mixture is defined as:

$$Z = \frac{Y_{\mathrm{CH4}}}{Y_{\mathrm{CH4}} + Y_{\mathrm{O2}}} \tag{3.5}$$

The solution is advanced in time using a typical time step of 1.7 ns, with a 0.8 CFL number. The simulations were performed using 480 Intel Xeon (E5-2698 v3) processors, and 17 μs of physical time could be completed in about an hour wall clock time.

4. Results

In the present study, two SGS models are investigated, namely the Vreman model and the Gradient model. The evaluation of the SGS terms from the momentum, energy, and mass fraction equations; τ_{ij}, q_i and j_i respectively; is described with equations (4.1) to (4.9).

The Vreman SGS model [1] belongs to a family of eddy-viscosity models:

$$\tau_{ij} = \widetilde{u_i u_j} - \widetilde{u}_i \widetilde{u}_j = -2\nu_{\mathrm{SGS}} \widetilde{S}_{ij} + \frac{1}{3}\tau_{kk}\delta_{ij} \tag{4.1}$$

where ν_{SGS} is the eddy viscosity, S_{ij} is the velocity strain tensor, and δ_{ij} is the Kronecker delta.

For the Vreman SGS model:

$$\nu_{\mathrm{SGS}} = C_v \sqrt{\frac{B}{a_{ij}a_{ij}}} \tag{4.2}$$

$$a_{ij} = \frac{\partial \widetilde{u}}{\partial x_j} \tag{4.3}$$

$$B = \beta_{11}\beta_{22} - \beta_{12}^2 + \beta_{11}\beta_{33} - \beta_{13}^2 + \beta_{22}\beta_{33} - \beta_{23}^2 \tag{4.4}$$

SGS Term	$\bar{\Delta} = 2\Delta$		$\bar{\Delta} = 4\Delta$	
(Vreman Model)	Slope	R^2	Slope	R^2
τ_{11}	0.891	0.0297	0.733	0.0261
τ_{22}	1.105	0.0463	0.675	0.0424
τ_{33}	0.973	0.0292	0.793	0.0213
τ_{12}	0.704	0.0396	0.685	0.0303
τ_{13}	0.869	0.0737	0.725	0.0630
τ_{23}	0.823	0.0693	0.714	0.0647
Mean	0.894	0.0480	0.721	0.0413

TABLE 2. Slopes and correlations from the least-square fit of the SGS stress terms from the Vreman Model and filtered DNS.

$$\beta_{ij} = \Delta_m^2 a_{mi} a_{mj} \tag{4.5}$$

where a Vreman Coefficient C_v of 0.07 has been used throughout this study.

Both subgrid-scale Prandtl number Pr_{SGS} and subgrid-scale Schmidt number Sc_{SGS} are set at a constant value of 0.9 for the evaluation of scalar SGS terms for simplicity. It should be noted that more complex scalar SGS models can be used in conjunction with the Vreman model for SGS stress, but the inclusion of which is beyond the scope of the current study.

$$q_i = \widetilde{u_i T} - \widetilde{u}_i \widetilde{T} = \frac{\nu_{\text{SGS}}}{Pr_{\text{SGS}}} \frac{\partial \widetilde{T}}{\partial x_i} \tag{4.6}$$

$$j_i = \widetilde{u_i Z} - \widetilde{u}_i \widetilde{Z} = \frac{\nu_{\text{SGS}}}{Sc_{\text{SGS}}} \frac{\partial \widetilde{Z}}{\partial x_i} \tag{4.7}$$

In addition, the Gradient model by Clark, Ferziger and Reynolds [15] has been considered:

$$\widetilde{u_i u_j} - \widetilde{u}_i \widetilde{u}_j = C_g \bar{\Delta}^2 \frac{\partial \widetilde{u}_i}{\partial x_k} \frac{\partial \widetilde{u}_j}{\partial x_k} \tag{4.8}$$

$$\widetilde{u_i \phi} - \widetilde{u}_i \widetilde{\phi} = C_g \bar{\Delta}^2 \frac{\partial \widetilde{u}_i}{\partial x_k} \frac{\partial \widetilde{\phi}}{\partial x_k} \tag{4.9}$$

where a coefficient C_g of 0.5 has been used throughout this study.

A priori analysis is performed by calculating the SGS terms from the filtered DNS data. The modeled SGS terms are then compared with the DNS results by using a least-squares fit.

The correlation, as represented by the coefficient of determination R^2, and slope for the least-squares regression model for the momentum SGS terms for the Vreman model and the Clark model at two different filter widths $\bar{\Delta}$ have been extracted and presented in tables 2 and 3. The mean slope from the Vreman fit is at 0.894 and 0.721 for $\bar{\Delta} = 2\Delta$ and $\bar{\Delta} = 4\Delta$ respectively, which indicates that the magnitude of the modeled SGS terms is in good agreement with the filtered DNS. However, poor correlation is seen with 0.0480 R^2 and 0.0413 R^2 values for the mesh resolution of $\bar{\Delta} = 2\Delta$ and $\bar{\Delta} = 4\Delta$ respectively, which is indicative of a large variation of errors. The Gradient Model demonstrates a good mean correlation with 0.896 and 0.721 R^2 values and adequate slope at 0.352

SGS Term	$\bar{\Delta} = 2\Delta$		$\bar{\Delta} = 4\Delta$	
(Gradient Model)	Slope	R^2	Slope	R^2
τ_{11}	0.347	0.879	0.322	0.733
τ_{22}	0.341	0.868	0.297	0.675
τ_{33}	0.369	0.924	0.326	0.793
τ_{12}	0.345	0.887	0.288	0.685
τ_{13}	0.355	0.913	0.302	0.725
τ_{23}	0.354	0.906	0.299	0.714
Mean	0.352	0.896	0.306	0.721

TABLE 3. Slopes and correlations from the least-square fit of the SGS stress terms from the Gradient Model and filtered DNS.

SGS Term	$\bar{\Delta} = 2\Delta$		$\bar{\Delta} = 4\Delta$	
(Vreman Model)	Slope	R^2	Slope	R^2
q_1	0.00197	0.0922	0.00195	0.0940
q_2	0.00152	0.0342	0.00159	0.0401
q_3	0.00194	0.0563	0.00185	0.0507
j_1	0.00313	0.1038	0.00274	0.1339
j_2	0.00320	0.0718	0.00265	0.0824
j_3	0.00298	0.0579	0.00212	0.0450
Mean	0.00246	0.0694	0.00215	0.0744

TABLE 4. Slopes and correlations from the least-square fit of the SGS scalar terms from the Vreman Model (with constant Pr_{SGS} and Sc_{SGS}) and filtered DNS.

and 0.306 for $\bar{\Delta} = 2\Delta$ and $\bar{\Delta} = 4\Delta$ respectively. It should be pointed out that the slope can be improved with the calibration of the model coefficients.

Figure 2(a) shows the scatter data and least-squares fit for the τ_{11} SGS term. The poor correlation is clear especially in comparison to the same plot for the Gradient model, shown in figure 2(b).

Similar trends in the correlation of the least-squares fit are seen for the scalar SGS terms as shown in tables 4 and 5. Poor mean correlation is observed from the Vreman model with 0.0694 and 0.0744 R^2 values for $\bar{\Delta} = 2\Delta$ and $\bar{\Delta} = 4\Delta$ respectively. On the other hand, good correlation is seen from the Gradient model with 0.875 and 0.707 R^2 values for $\bar{\Delta} = 2\Delta$ and $\bar{\Delta} = 4\Delta$ respectively. Contrary to the momentum SGS term, the mean slope from the scalar SGS terms are poor with 0.00246 and 0.00215 values for $\bar{\Delta} = 2\Delta$ and $\bar{\Delta} = 4\Delta$ respectively. This is likely due to the use of constant Pr_{SGS} and Sc_{SGS} in evaluating the scalar SGS terms, which is unsuitable due to the large range of temperature and density within the domain. On the other hand, the mean slope of the Gradient Model for the scalar SGS terms remains similar with the momentum SGS terms at 0.335 and 0.267 R^2 values for $\bar{\Delta} = 2\Delta$ and $\bar{\Delta} = 4\Delta$ respectively.

To study the difference in performance between the two models, the Boussinesq hy-

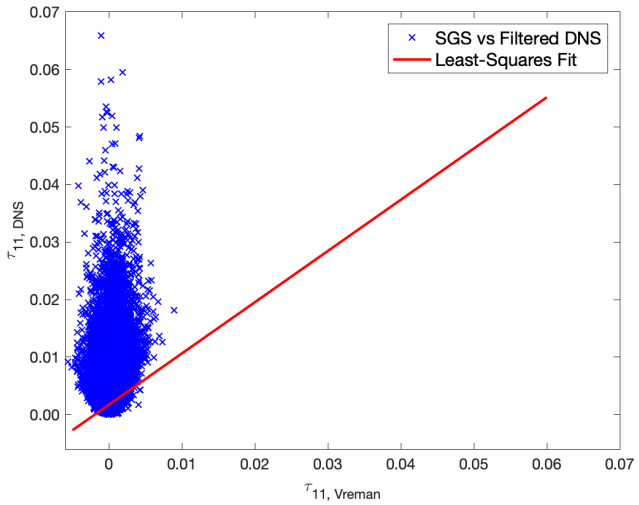

(a) $\tau_{11,\text{DNS}}$ vs $\tau_{11,\text{Vreman}}$.

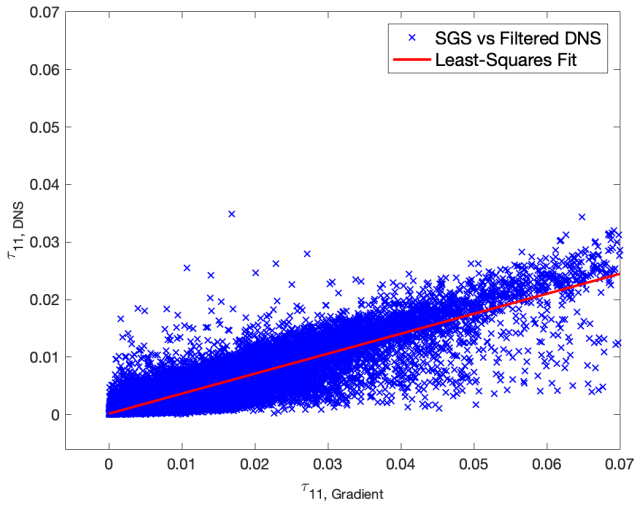

(b) $\tau_{11,\text{DNS}}$ vs $\tau_{11,\text{Gradient}}$.

FIGURE 2. Least-squares fit of the filtered DNS momentum SGS term $\tau_{11,\text{DNS}}$ vs modeled model SGS term $\tau_{11,\text{model}}$.

pothesis is tested by taking the dot product of the diagonal momentum SGS tensor and the strain tensor. By inspecting eq. (4.1), if the momentum subgrid-scale terms obeyed the Boussinesq hypothesis, then the angle θ between the diagonal of the subgrid-scale tensor τ_{ii} and the diagonal of the strain tensor $\dfrac{\partial \widetilde{u}_i}{\partial x_i}$ will be 0° or 180°. This can be expressed via the dot product:

$$\tau_{ii} \cdot \frac{\partial \widetilde{u}_i}{\partial x_i} = |\tau_{ii}| \left| \frac{\partial \bar{u}_i}{\partial x_i} \right| \cos\theta \tag{4.10}$$

SGS Term	$\bar{\Delta} = 2\Delta$		$\bar{\Delta} = 4\Delta$	
(Gradient Model)	Slope	R^2	Slope	R^2
q_1	0.313	0.811	0.230	0.608
q_2	0.335	0.826	0.272	0.628
q_3	0.376	0.915	0.305	0.745
j_1	0.314	0.870	0.236	0.700
j_2	0.317	0.867	0.263	0.724
j_3	0.354	0.957	0.296	0.837
Mean	0.335	0.875	0.267	0.707

TABLE 5. Slopes and correlations from the least-square fit of the SGS scalar terms from the Gradient Model and filtered DNS.

Figure 3(a) compares the polar probability density function (PDF) plot of (4.10), between SGS terms from filtered DNS data and the Vreman model, with the magnitude as the radial axis and the angle between the vectors as the azimuthal axis. It can be seen that the radial maximum of filtered DNS on the left half of the PDF plot is in good agreement with the Vreman SGS terms on the right. This is in good agreement with table 2 where the slopes of the Vreman terms are close to unity. However, the shapes of the contour plots between the two differ – all of the Vreman terms are at 180°, due to the Boussinesq hypothesis, while the filtered DNS terms possess a bimodal shape with modes at approximately 60° and 120°. This discrepancy suggests that SGS models that utilize the eddy-viscosity hypothesis may be unsuitable in transcritical mixtures.

Figure 3(b) shows that the contour from the Gradient SGS agrees in shape with the contour from the filtered DNS data. However, the magnitude of the Gradient SGS terms in the radial direction are approximately three times larger than the filtered DNS equations. This matches the slopes of approximately 0.3 in table 3. These results indicate that the Gradient SGS model may be suitable in the LES of transcritical flow, provided that the terms are scaled correctly. However, it should be pointed out that the Gradient model has been known to perform better in *a priori* analysis than in *a posteriori* analysis [16]. Nonetheless, these results suggest that methods that capture SGS behaviour that deviate from the Boussinesq hypothesis, including the present Gradient model and other methods such as the Regularized Deconvolution Method [10], may be suitable for transcritical flows.

5. Conclusions and Future Work

DNS of an inert transcritical LOX-GCH4 mixture was performed. *A priori* analysis was then conducted on the favre-filtered DNS data to determine the suitability of two common SGS models in transcritical flows. Ambient pressure and species temperature was chosen to match conditions in a LOX-GCH4 rocket combustor. Homogeneous isotropic turbulence is used as the initial flow field. The simulation is run until the flow field resembled realistic turbulence, and the fluid was allowed to mix under these conditions.

A priori analysis showed that the SGS terms evaluated by Vreman SGS model correlated poorly with the SGS terms from filtered DNS. In contrast, good correlation is seen between the terms from the Gradient SGS model and the filtered DNS data. Probability

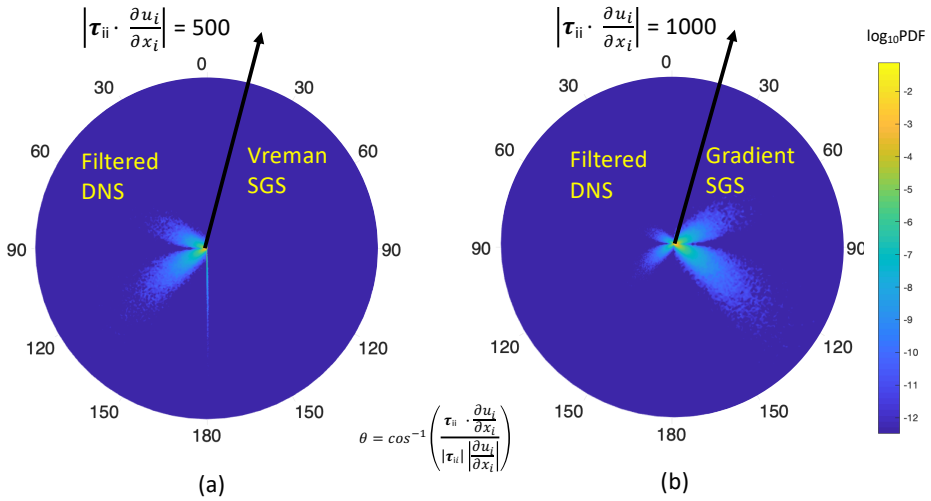

FIGURE 3. PDF plot of the diagonals of the dot product of SGS stress tensor and the viscous strain tensor.

density function plots of the scalar product of terms from the SGS stress tensor and viscous strain tensor has been used to demonstrate that Gradient Model is able to capture the deviation of the subgrid-scale terms from the Boussinesq hypothesis, while the Vreman SGS model, which is based on eddy viscosity concepts is inadequate.

Additional future work include repeating the present analysis on a reacting case under the same conditions. Moreover, the present study should be repeated with an *a posteriori* study to generate further insight.

Acknowledgments

Financial support has been provided by the German Research Foundation (Deutsche Forschungsgemeinschaft – DFG) in the framework of the Sonderforschungsbereich Transregio 40.

References

[1] VREMAN, A.W. (2004). An eddy-viscosity subgrid-scale model for turbulent shear flow: Algebraic theory and applications. *Physics of Fluids*, **16**(10), 3670–3681.

[2] MA, P.C., LV, Y. AND IHME, M. (2017). An entropy-stable hybrid scheme for simulations of transcritical real-fluid flows. *Journal of Computational Physics*, **340**, 330–357.

[3] ABGRALL, R. AND KARNI, S. (2001). Computations of compressible multifluids. *Journal of Computational Physics*, **169**(2), 594–623.

[4] CHUNG, T.H., AJLAN, M., LEE, L.L. AND STARLING, K.E. (1988). Generalized multiparameter correlation for nonpolar and polar fluid transport properties. *Industrial & Engineering Chemistry Research*, **27**(4), 671–679.

[5] SELLE, L.C., OKONG'O, N.A., BELLAN, J. AND HARSTAD, K.G. (2007). Modelling of subgrid-scale phenomena in supercritical transitional mixing layers: an a priori study. *Journal of Fluid Mechanics*, **593**, 57–91.

[6] TAKAHASHI, S. (1975). Preparation of a generalized chart for the diffusion coefficients of gases at high pressures. *Journal of Chemical Engineering of Japan*, **7**(6), 417–420.

[7] POLING, B.E., PRAUSNITZ, J.M. AND O'CONNELL, J.P. (2001). *The Properties of Gases and Liquids*. McGraw-Hill.

[8] KHALIGHI, Y., NICHOLS, J.W., LELE, S.K., HAM, F. AND MOIN, P. (2011). Unstructured large eddy simulation for prediction of noise issued from turbulent jets in various configurations. In: *AIAA Paper 2011-2886*.

[9] RICHARDS, A., SUTHERLAND, J.C. AND SAAD, T. (2018). A fast turbulence generator using graphics processing units. In: *AIAA Paper 2018-3559*.

[10] WANG, Q. AND IHME, M. (2019). A regularized deconvolution method for turbulent closure modeling in implicitly filtered large-eddy simulation. *Combustion and Flame*, 341–355.

[11] BAILLY, C. AND JUVES, D. (1999). A stochastic approach to compute subsonic-noise using linearized Euler's equations. In: *AIAA Paper 99-1872*.

[12] RIBERT, G., DOMINGO, P. AND VERVISCH, L. (2019). Analysis of sub-grid scale modeling of the ideal-gas equation of state in hydrogen-oxygen premixed flames. *Proceedings of the Combustion Institute*, **37**(2), 2345–2351. ISSN 15407489. DOI 10.1016/j.proci.2018.07.054.

[13] SAAD, T. AND SUTHERLAND, J.C. (2016). Comment on "Diffusion by a random velocity field" [Phys. Fluids 13, 22 (1970)]. *Physics of Fluids*, **28**(11).

[14] WILLIAMS, F. (2006). Descriptions of nonpremixed turbulent combustion. In: *AIAA Paper 2006-1505*.

[15] CLARK, R.A., FERZIGER, J.H. AND REYNOLDS, W.C. (1979). Evaluation of subgrid-scale models using an accurately simulated turbulent flow. *Journal of Fluid Mechanics*, **91**(1), 1–16.

[16] VREMAN, B., GEURTS, B. AND KUERTEN, H. (2019). Large-eddy simulation of the turbulent mixing layer. *Journal of Fluid Mechanics*, **339**, 357–390.

[17] SAAD, T., CLINE, D., STOLL, R. AND SUTHERLAND, J.C. (2017). Scalable tools for generating synthetic isotropic turbulence with arbitrary spectra. *AIAA Journal*, **55**(1), 327–331.